International Journal of Numerical Methods for Heat & Fluid Flow

Finite element modeling of nonlinear reaction-diffusion-advection systems of equations

Sanjay Komala Sheshachala, Ramon Codina,

Finite element modeling of nonlinear reaction–diffusion–advection systems of equations

Sanjay Komala Sheshachala
College of Engineering, Swansea University, Swansea, UK, and
Ramon Codina
Department of Civil and Environmental Engineering, Technical University of Catalonia, Barcelona, Spain

Received 26 February 2018
Revised 25 May 2018
Accepted 25 May 2018

Abstract

Purpose – This paper aims to present a finite element formulation to approximate systems of reaction–diffusion–advection equations, focusing on cases with nonlinear reaction. The formulation is based on the orthogonal sub-grid scale approach, with some simplifications that allow one to stabilize only the convective term, which is the source of potential instabilities. The space approximation is combined with finite difference time integration and a Newton–Raphson linearization of the reactive term. Some numerical examples show the accuracy of the resulting formulation. Applications using classical nonlinear reaction models in population dynamics are also provided, showing the robustness of the approach proposed.

Design/methodology/approach – A stabilized finite element method for advection–diffusion–reaction equations to the problem on nonlinear reaction is adapted. The formulation designed has been implemented in a computer code. Numerical examples are run to show the accuracy and robustness of the formulation.

Findings – The stabilized finite element method from which the authors depart can be adapted to problems with nonlinear reaction. The resulting method is very robust and accurate. The framework developed is applicable to several problems of interest by themselves, such as the predator–prey model.

Originality/value – A stabilized finite element method to problems with nonlinear reaction has been extended. Original contributions are the design of the stabilization parameters and the linearization of the problem. The application examples, apart from demonstrating the validity of the numerical model, help to get insight in the system of nonlinear equations being solved.

Keywords Nonlinear reaction, Predator–prey model, Stabilized finite element methods

Paper type Research paper

1. Introduction

Nonlinear reaction–diffusion equations are encountered in modeling of a variety of phenomena, such as nonuniform chemical reactions (Cussler, 2013), propagation of nerve pulses in a neuron (Nagumo *et al.*, 1962), circuit theory in electronic design (Linares-Barranco *et al.*, 1991) and rumor spreading in sociology (Zhu *et al.*, 2016). These equations were first arrived at simultaneously by Fisher (1937) and the team of Kolmogorov, Petrovsky and Piskunov (KPP) (Tikhomirov, 1991) to model population densities in ecology. They exhibit properties that are well studied, such as formation of spatio-temporal patterns, traveling waves and bifurcation (Tikhomirov, 1991). See (Kawasaki, 1997), for an intuitive explanation of nonlinear reaction–diffusion equations for population models.

Of particular interest is the application of nonlinear reaction–diffusion equations in the modeling of predator–prey interactions. Medvinsky *et al.* (2002) studied plankton and fish population dynamics through such a model. A logistic growth for prey and Hollinger type II

International Journal of Numerical Methods for Heat & Fluid Flow

0961-5539
DOI 10.1108/HFF-02-2018-0077

functional response for predator species, together called the Rosenzweig–MacArthur form, were used. Garvie *et al.* (2015) used the same predator–prey model and proposed a finite element method to solve it. The emphasis was placed on elaborating the effects of non-standard habitat shape, initial and boundary conditions on the solution.

Advection terms in population models are used to incorporate foraging strategies exhibited by species. The study by Grünbaum (1999) mimics population-level flux of organisms toward regions of better resources based on local clues through advection terms. Phytoplankton growth with advection in a heterogeneous environment was demonstrated by Ryabov and Blasius (2008). Murray (2007) suggested that nonlinear diffusion can be thought of as contributing to an equivalent advection term. However, the most natural way to introduce advection in a reaction–diffusion model is to introduce the effect of the transport of the quantity of interest in a fluid flow. In this case, the need to extend classical nonlinear reaction–diffusion models to reaction–diffusion–advection (RDA) models is obvious.

Referring to the numerical approximation, the Galerkin finite element method applied to the RDA equation fails to yield a meaningful solution if either the advection term or the reaction term is large relative to the diffusion term. To elaborate this, consider a linear, transient RDA equation. The quantity of interest u, assumed to be scalar, is the solution in a domain Ω (in 2D or 3D) of the problem:

$$\frac{\partial u}{\partial t} - \nabla \cdot \mathbf{K} \cdot \nabla u + \mathbf{a} \cdot \nabla u + su = f \text{ in } \Omega, \quad t > 0 \tag{1}$$

$$u = u_0 \text{ in } \Omega, \quad t = 0 \tag{2}$$

$$u = u_D \text{ on } \partial\Omega_D, \quad t > 0 \tag{3}$$

$$\mathbf{n} \cdot \boldsymbol{K} \cdot \nabla u = g_N \text{ on } \partial\Omega_N, \quad t > 0 \tag{4}$$

Here, $\boldsymbol{K}$ is the diffusion tensor, which we will assume positive definite throughout; $\boldsymbol{a}$ is the advective velocity, which we will consider divergence free throughout; $s \geq 0$ is the reaction coefficient; and f is the source term. The initial condition u_0 for the RDA equation has to be specified. The boundary of the domain $\partial\Omega$ is assumed to be made up of Dirichlet $\partial\Omega_D$ and Neumann $\partial\Omega_N$ parts, such that $\partial\Omega = \partial\Omega_D \cup \partial\Omega_N$ and $\partial\Omega_D \cap \partial\Omega_N = \emptyset$. Boundary conditions of the Dirichlet u_D and Neumann g_N kind are specified on the respective boundaries.

Following the finite element procedure, let the domain Ω be discretized into a collection of elements $\{K\}$ with a characteristic length h. Quasi-uniform meshes are assumed, for simplicity.

For the problem we consider, the non-dimensional quantities of significance are the numerical Péclet number Pe and Damköhler number Da, defined as:

$$\text{Pe} = \frac{|\mathbf{a}|h}{2k}, \qquad \text{Da} = \frac{sh^2}{k}$$

where k is a characteristic value of the diffusion tensor (for example the minimum eigenvalue). The numerical Péclet number is a measure of the relative strength of convection

to that of diffusion, and the Damköhler number is a measure of relative strength of reaction to that of diffusion. Standard Galerkin finite element methods fail when $\mathrm{Pe} > 1$ or $\mathrm{Da} \gg 1$, giving rise to oscillatory solutions. These oscillations may be removed using the so-called stabilized finite element methods.

Various stabilization schemes can be applied to the finite element approximation of the problem we consider, such as the Galerkin least squares method, the streamline upwind Petrov Galerkin method and the Taylor Galerkin method. These methods use different ways of adding numerical diffusion, and were brought under the umbrella of a single theoretical framework by Hughes (1995), which introduced the concept of sub-grid scale model. Each one of the stabilization techniques that had appeared earlier in the literature was shown to arise from a particular class of sub-grid scale model as suggested by Hughes *et al.* (1998) and elucidated in Codina (1998).

The remedy we propose in this work is to add stabilization, particularly, the least diffusive orthogonal sub-grid scale (OSS) stabilization developed by Codina (2002), which in turn is based on variational multi-scale (VMS) methods proposed by Hughes (1995). The basic idea of the VMS approach is that the solution u can be evaluated as the sum of the two components $u = \overline{u} + \tilde{u}$. $\overline{u}$ is the so-called coarse grid solution, which is typically approximated numerically using the finite element method and $\tilde{u}$ is the so-called fine grid solution or sub-grid scale, which is determined analytically *a priori* in terms of $\overline{u}$. The idea is to obtain the "effect" of $\tilde{u}$ on $\overline{u}$ rather than an explicit expression for $\tilde{u}$. Therefore, a good design of the sub-grid scale solution is the logical next step. The relationship between the coarse grid and the sub-grid component plays a major role in this process. OSS stabilization in particular uses the sub-grid scale orthogonal to the residual of the finite element coarse grid solution as a correction term.

In the following sections, the OSS stabilization formulation is introduced and applied to stand-alone and coupled transient, nonlinear RDA equations. Later, results from the numerical tests to check the accuracy and convergence using the method of manufactured solutions are discussed. Furthermore, results from the numerical method applied to the Fisher–KPP model and the aforementioned predator–prey model with Rosenzweig–MacArthur reaction terms are presented. Even if simple geometries will be used, we would like to stress that the formulation presented is applicable to any domain; this flexibility to handle complex geometries is one of the main advantages of the finite element method.

For the numerical methods community, this paper expands the use of the OSS stabilization to nonlinear RDA systems of equations, and for the mathematical modeling community, it presents a usable method for tackling large advection and reaction terms in RDA equations and demonstrates it for population models.

2. Problem statement

Consider the following general system of n_{unk} coupled transient nonlinear RDA equations, subjected for simplicity to homogeneous Dirichlet boundary conditions and to an initial condition $\boldsymbol{U}^0$:

$$\frac{\partial \boldsymbol{U}}{\partial t} - \mathcal{L}(\boldsymbol{U}) = \boldsymbol{F} \qquad \text{in} \quad \Omega, \ t > 0 \tag{5}$$

$$\boldsymbol{U} = \boldsymbol{0} \qquad \text{on } \partial\Omega, \ t > 0 \tag{6}$$

$$\boldsymbol{U} = \boldsymbol{U}^0 \qquad \text{in}\,\Omega,\ t = 0 \tag{7}$$

where

$$\mathcal{L}(\boldsymbol{U}) := -\frac{\partial}{\partial x_i}\left(\boldsymbol{K}_{ij}\frac{\partial \boldsymbol{U}}{\partial x_j}\right) + \frac{\partial}{\partial x_i}(\boldsymbol{A}_i\boldsymbol{U}) + \mathrm{SU}$$

Here, n_{unk} is the number of equations/unknowns in the system, Ω is the computational domain of n_{sd} spatial dimensions and coordinates x_i, $\boldsymbol{U}$ and $\boldsymbol{F}$ are vectors of n_{unk} unknowns and sources respectively and $\boldsymbol{A}_i$, $\boldsymbol{K}_{ij}$ and $\boldsymbol{S}$ are $n_{\mathrm{unk}} \times n_{\mathrm{unk}}$ matrices ($i,j = 1, \ldots, n_{sd}$). Einstein summation convention is assumed.

In our applications, we will be interested in cases in which diffusion and advection coefficients are linear and the coupling of the system is through the nonlinear reaction coefficients only. Hence, $\boldsymbol{A}_i = \mathrm{diag}((a_i)_{1,\ldots,}(a_i)_{n_{unk}})$, where $(a_i)_J$ is the constant scalar advection component in the i-th spatial direction for the J-th equation in the system. Likewise, we will consider cases with isotropic diffusion for each component of the unknown, so that $K_{ij} = \boldsymbol{K}_d\delta_{ij}$, $i, j = 1,\ldots n_{sd}$, with $\boldsymbol{K}_d = \mathrm{diag}(k_1, \ldots, k_{n_{\mathrm{unk}}})$. The nonlinear reaction coefficients are $s_{IJ}(\boldsymbol{U})$ where $I, J = 1,\ldots, n_{unk}$. The treatment of these terms is the main focus of this paper.

To simplify the exposition, we have considered homogeneous Dirichlet conditions for all components of the vector of unknowns. This is possible if we consider $k_I > 0$, $I = 1,\ldots, n_{unk}$. Nevertheless, the discussion below can be easily extended to cases in which some components have zero diffusion, cases in which Dirichlet boundary conditions can only be specified at inflows or cases in which some components have Neumann-type conditions of the form (4).

Let us write down the weak form of equations (5)-(7). Let $\mathcal{V} = \left(H_0^1(\Omega)\right)^{n_{\mathrm{unk}}}$, which is defined as $\left(H_0^1(\Omega)\right)^{n_{\mathrm{unk}}} = \{\boldsymbol{U} | U_J \in L^2(\Omega), \nabla U_J \in \left(L^2(\Omega)\right)^{n_{\mathrm{sd}}}$ and $U_J = 0$ on $\partial\Omega\ \forall J = 1, \ldots, n_{\mathrm{unk}}\}$. If $[0,\ T]$ is the time interval of analysis, the problem consists in finding $\boldsymbol{U} : [0,\ T] \to \mathcal{V}$ such that:

$$\left(\frac{\partial \boldsymbol{U}}{\partial t}, \boldsymbol{V}\right) + B(\boldsymbol{V}, \boldsymbol{U}) = \langle \boldsymbol{V}, \boldsymbol{F}\rangle \qquad \forall \boldsymbol{V} \in \mathcal{V} \tag{8}$$

$$\left(\boldsymbol{U}|_{t=0}, \boldsymbol{V}\right) = \left(\boldsymbol{U}^0, \boldsymbol{V}\right) \qquad \forall \boldsymbol{V} \in \mathcal{V} \tag{9}$$

where

$$B(\boldsymbol{V}, \mathrm{U}) := \int_\Omega \boldsymbol{V}^T \frac{\partial}{\partial x_i}(\boldsymbol{A}_i\boldsymbol{U})\,\mathrm{d}\Omega + \int_\Omega \frac{\partial \boldsymbol{V}^T}{\partial x_i}\boldsymbol{K}_{ij}\frac{\partial \boldsymbol{U}}{\partial x_j}\,\mathrm{d}\Omega + \int_\Omega \boldsymbol{V}^T\boldsymbol{S}\boldsymbol{U}\,\mathrm{d}\Omega$$

$$\langle \boldsymbol{V}, \boldsymbol{F}\rangle := \int_\Omega \boldsymbol{V}^T\boldsymbol{F}\,\mathrm{d}\Omega$$

Here $(\cdot,\cdot)$ is the $L^2(\Omega)$ inner product and $<\cdot,\cdot>$ is the integral over Ω of product of two functions.

3. Numerical approximation

A formulation suited for the system of RDA equations introduced above is presented next. Recall that we have considered that the nonlinearity is present in the reaction term only. We will start describing the stabilized finite element method used to avoid oscillations when

diffusion is small. It is based on the OSS formulation (Codina, 2002, 2000; Codina and Blasco, 2002) for systems of equations, with some simplifications. The particular way to deal with the nonlinear reactive term will be indicated for each application in the following sections.

3.1 Stabilized finite element formulation

For the sake of simplicity, let us consider the approximation of the stationary form of equation (8). When a finite element solution is sought, the solution space is $\mathcal{V}_h \subset \mathcal{V}$, which is built from a partition $\mathcal{P} = \{K\}$ of the domain Ω. Using the Galerkin finite element formulation, now the problem can be stated as follows:

$$\text{Find } \boldsymbol{U}_h \in \mathcal{V}_h \text{ such that} \qquad B(\boldsymbol{V}_h, \boldsymbol{U}_h) = \langle \boldsymbol{V}_h, \boldsymbol{F} \rangle \quad \forall \boldsymbol{V}_h \in \mathcal{V}_h$$

Let us describe the VMS concept. We decompose the solution $\boldsymbol{U}$ into the component solved by finite element approximation $\boldsymbol{U}_h$ and the unresolvable component $\tilde{\mathbf{U}}$. As a result, the solution space now becomes $\mathcal{V} = \mathcal{V}_h \oplus \tilde{\mathcal{V}}$. Two equations arise from testing the weak form with test functions $\boldsymbol{V}_h$ and $\tilde{\boldsymbol{V}}$, namely:

$$B(\boldsymbol{V}_h, \boldsymbol{U}_h) + B\big(\boldsymbol{V}_h, \tilde{\boldsymbol{U}}\big) = \langle \boldsymbol{V}_h, \boldsymbol{F} \rangle \quad \forall \boldsymbol{V}_h \in \mathcal{V}_h \tag{10}$$

$$B\big(\tilde{\boldsymbol{V}}, \boldsymbol{U}_h\big) + B\big(\tilde{\boldsymbol{V}}, \tilde{\boldsymbol{U}}\big) = \langle \tilde{\boldsymbol{V}}, \boldsymbol{F} \rangle \quad \forall \tilde{\boldsymbol{V}} \in \tilde{\mathcal{V}} \tag{11}$$

Using the definition of adjoint operator $\mathcal{L}^*$ and that $B(\boldsymbol{V}, \boldsymbol{U}) = \langle \boldsymbol{V}, \mathcal{L}\boldsymbol{U} \rangle = \langle \mathcal{L}^* \boldsymbol{V}, \boldsymbol{U} \rangle$ (in the distributional sense), the equations become:

$$B(\boldsymbol{V}_h, \boldsymbol{U}_h) + \langle \mathcal{L}^* \boldsymbol{V}_h, \tilde{\boldsymbol{U}} \rangle = \langle \boldsymbol{V}_h, \boldsymbol{F} \rangle \quad \forall \boldsymbol{V}_h \in \mathcal{V}_h \tag{12}$$

$$\langle \tilde{\boldsymbol{V}}, \mathcal{L}\boldsymbol{U}_h \rangle + \langle \tilde{\boldsymbol{V}}, \mathcal{L}\tilde{\boldsymbol{U}} \rangle = \langle \tilde{\boldsymbol{V}}, \boldsymbol{F} \rangle \quad \forall \tilde{\boldsymbol{V}} \in \tilde{\mathcal{V}} \tag{13}$$

Two approximations to the sub-grid scale component $\tilde{\boldsymbol{U}}$ are now introduced. First, the jumps of the solution derivatives across the element boundaries are assumed to be zero. But this is not a necessary approximation, as shown by Codina *et al.* (2009), where it is explained that the choice of sub-grid scale must be able to satisfy the condition that the value of sub-grid scales at the element boundaries should be proportional to the jump of the flux of the finite element component and the average of the sub-grid scale value in the element interior. Nevertheless, with the approximation mentioned, we have:

$$\langle \tilde{\boldsymbol{V}}, \mathcal{L}\boldsymbol{U}_h \rangle \approx \sum_K \big(\tilde{\boldsymbol{V}}, \mathcal{L}\boldsymbol{U}_h\big)_K \equiv \big(\tilde{\boldsymbol{V}}, \mathcal{L}\boldsymbol{U}_h\big)_h$$

where $(\cdot,\cdot)_K$ denotes the product of the integral of two functions over the element domain K. Similarly, $\langle \mathcal{L}\boldsymbol{V}_h, \tilde{\boldsymbol{U}} \rangle \approx \big(\mathcal{L}\boldsymbol{V}_h, \tilde{\boldsymbol{U}}\big)_h$.

The second approximation is the crucial one, and can be expressed as follows:

$$\langle \tilde{\boldsymbol{V}}, \mathcal{L}\tilde{\boldsymbol{U}} \rangle = \big(\tilde{\boldsymbol{V}}, \boldsymbol{\tau}^{-1}\tilde{\boldsymbol{U}}\big)$$

where $\boldsymbol{\tau}$ is called the matrix stabilization parameters and is defined in equation (14) below. Its design is the bottleneck of stabilized finite element methods. See the studies of Codina (1998, 2000)

and Principe and Codina (2010) for a discussion about possible ways to obtain it. In our case, due to the assumptions made for the convection and diffusion coefficients, we may adopt a diagonal expression for $\boldsymbol{\tau}$ of the form $\boldsymbol{\tau} = \text{diag}(\tau_1, \ldots, \tau_{n_{\text{unk}}})$, where the J-th entry is:

$$\tau_J^{-1} = c_1 \frac{k_J}{h^2} + c_2 \frac{|\boldsymbol{a}_J|}{h} + c_3 s_J^* \tag{14}$$

where c_1, c_2 and c_3 are algorithmic constants and s_J^* is a characteristic reaction value to be specified for each particular reactive term. For linear finite elements, we take $c_1 = 4$, $c_2 = 2$, $c_3 = 1$.

With the approximations described, the equations now become:

$$B(\boldsymbol{V}_h, \boldsymbol{U}_h) + \left(\mathcal{L}^* \boldsymbol{V}_h, \tilde{\boldsymbol{U}}\right)_h = \langle \boldsymbol{V}_h, \boldsymbol{F} \rangle \quad \forall \boldsymbol{V}_h \in \mathcal{V}_h \tag{15}$$

$$\left(\tilde{\boldsymbol{V}}, \mathcal{L}\boldsymbol{U}_h\right)_h + \left(\tilde{\boldsymbol{V}}, \boldsymbol{\tau}^{-1}\tilde{\boldsymbol{U}}\right) = \langle \tilde{\boldsymbol{V}}, \boldsymbol{F} \rangle \quad \forall \tilde{\boldsymbol{V}} \in \tilde{\mathcal{V}} \tag{16}$$

The sub-grid space is yet to be defined and it may not belong to $\left(H_0^1(\Omega)\right)^{n_{\text{unk}}}$. From equation (16), it is seen that the sub-grid solution is composed of the L^2 projection onto the space $\tilde{\mathcal{V}}$ (denoted by $\tilde{\mathcal{P}}$) of the residual of the finite element solution multiplied by $\boldsymbol{\tau}$:

$$\tilde{\boldsymbol{U}} = \boldsymbol{\tau}\tilde{\mathcal{P}}(\boldsymbol{F} - \mathcal{L}\boldsymbol{U}_h)$$

In the OSS stabilization, the sub-grid space is taken as orthogonal to the finite element space $\mathcal{V}_h$, that is to say:

$$\tilde{\mathcal{V}} = \mathcal{V}_h^{\perp}, \qquad \tilde{\boldsymbol{U}} = \boldsymbol{\tau}\mathcal{P}_h^{\perp}(\boldsymbol{F} - \mathcal{L}\boldsymbol{U}_h) \tag{17}$$

where $\mathcal{P}_h^{\perp} = I - \mathcal{P}_h$ and $\mathcal{P}_h$ is the L^2 projection onto the finite element space.

This is the general expression of the OSS method. However, further simplifications can be done. For the problem we consider, one that simplifies considerably the method is to consider the advective component of the residual alone. This is enough for stability because the Galerkin formulation precisely lacks control over the component of the advective term $\frac{\partial(\boldsymbol{A}_i \mathbf{U})}{\partial x_i}$ orthogonal to the finite element space. From the accuracy point of view, the orthogonal component of this advective term is expected to be of the same order as the finite element interpolation, and therefore optimal (see for example the analysis in Codina and Blasco [2002]). This is in contrast to the algebraic sub-grid scale choice, in which $\tilde{\boldsymbol{U}} = \boldsymbol{\tau}(\boldsymbol{F} - \mathcal{L}\boldsymbol{U}_h)$, i.e. $\tilde{\mathcal{P}}$ is the identity on finite element residuals; the finite element approximation in this case tends to be more diffusive. Note that for constant reaction coefficients, the orthogonal projection of the reactive term is zero exactly, but for nonlinear reaction, neglecting it is equivalent to say that this nonlinear (continuous) term is approximated by a finite element function.

With the approximations described, we have that:

$$\tilde{\boldsymbol{U}} = -\boldsymbol{\tau}\mathcal{P}_h^{\perp}\left(\frac{\partial(\boldsymbol{A}_i \boldsymbol{U}_h)}{\partial x_i}\right) \tag{18}$$

which upon substitution into equation (15) leads to the following:

$$B(\boldsymbol{V}_h, \boldsymbol{U}_h) + \left(\mathcal{L}^* \boldsymbol{V}_h, -\tau \mathcal{P}_h^{\perp} \left(\frac{\partial (\boldsymbol{A}_i \boldsymbol{U}_h)}{\partial x_i} \right) \right)_h = \langle \boldsymbol{V}_h, \boldsymbol{F} \rangle \qquad \forall \boldsymbol{V}_h \in \mathcal{V}_h \tag{19}$$

The formal adjoint $\mathcal{L}^*$ is given by:

$$\mathcal{L}^* \boldsymbol{V}_h = -\frac{\partial}{\partial x_i} \left(\boldsymbol{K}_{ij}^T \frac{\partial \boldsymbol{V}_h}{\partial x_j} \right) - \boldsymbol{A}_i^T \frac{\partial \boldsymbol{V}_h}{\partial x_i} + \boldsymbol{S}^T \boldsymbol{V}_h$$

Of these three terms, only the second one yields stability when tested against equation (18). The first one is zero for constant diffusion and linear elements and the third one is zero when tested against equation (18) for constant reaction. In any case, we may keep only the second term (we may use any operator on the test function and keep the original accuracy of the formulation). Moreover, only the component orthogonal to the finite element space remains when tested by equation (18). Therefore, the final form of the method we propose is:

$$B(\boldsymbol{V}_h, \boldsymbol{U}_h) + \left(\mathcal{P}_h^{\perp} \left(\boldsymbol{A}_i^T \frac{\partial \boldsymbol{V}_h}{\partial x_i} \right), \tau \mathcal{P}_h^{\perp} \left(\frac{\partial (\boldsymbol{A}_i \boldsymbol{U}_h)}{\partial x_i} \right) \right)_h = \langle \boldsymbol{V}_h, \boldsymbol{F} \rangle \qquad \forall \boldsymbol{V}_h \in \mathcal{V}_h. \tag{20}$$

The OSS formulation provides global stability bounds for the solution, but not local ones, since the method lacks monotonicity. Hence only global convergence is guaranteed. Typically, oscillations are restricted to only a few layers around sharp gradients. This is easily mitigated by using shock-capturing techniques or selective mesh refinement, even though we will not touch these topics in this work. The meshes used in the numerical examples are fine enough to avoid local oscillations.

3.2 Finite element implementation

Let us describe a few aspects of the finite element implementation of the formulation presented. Let us assume that the finite element mesh is composed of n_p nodes and let us denote with a superscript a the nodal values of a function at node a. The shape function at this node will be $\mathrm{N}^a = \mathrm{N}^a(\boldsymbol{x})$. Assuming equal interpolation for all the unknowns, the solution $\boldsymbol{U}_h$ of equation (20) and the test function $\boldsymbol{V}_h$ in this equation can be expressed in terms of the nodal values $\mathbf{U}^a$ and $\mathbf{V}^a$, respectively, as:

$$\boldsymbol{U}_h = \sum_{a=1}^{n_{\mathrm{p}}} \mathbf{U}^a \mathrm{N}^a, \qquad \boldsymbol{V}_h = \sum_{b=1}^{n_{\mathrm{p}}} \mathbf{U}^b \mathrm{N}^b$$

Some of the components of the unknowns are given by the Dirichlet boundary conditions. The equations corresponding to these unknowns may be deleted before solving the final algebraic system. This resulting algebraic form of equation (20) for the stationary nonlinear RDA equation is:

$$\left(\mathbf{K}_k + \mathbf{K}_a + \mathbf{K}_s(\mathbf{U}) + \mathbf{K}_{\mathrm{oss}} \right) \mathbf{U} = \mathbf{F} \tag{21}$$

where the diffusion matrix $\mathbf{K}_k$, the advection matrix $\mathbf{K}_a$ and the reaction matrix $\mathbf{K}_s$ are of dimension ($n_p\ n_{uk} \times n_p\ n_{uk}$) and the source vector $\mathbf{F}$ is of dimension ($n_p\ n_{uk}$). We

have explicitly indicated that the only nonlinear term we consider is the reactive one. $\mathbf{K}_k$ and $\mathbf{K}_a$ are block diagonal matrices, with each block of dimension $(n_p \times n_p)$ defined below:

$$\mathbf{K}_k|_J^{ab} = k_J \int_\Omega \nabla \mathrm{N}^b \cdot \nabla \mathrm{N}^a \mathrm{d}\Omega, \qquad a, b = 1, \ldots, n_\mathrm{p}$$
$$\mathbf{K}_a|_J^{ab} = \int_\Omega \mathrm{N}^b \left(\boldsymbol{a}_J \cdot \nabla \mathrm{N}^a\right) \mathrm{d}\Omega, \qquad a, b = 1, \ldots, n_\mathrm{p}$$

where $J = 1,\ldots, n_{unk}$.

As the nonlinearity and coupling of the system is through the reaction term, the reaction matrix is a full matrix consisting of $n_p\ n_{uk}$ rows and $n_p\ n_{uk}$ columns, the components of which are given by:

$$\mathbf{K}_s|_{IJ}^{ab} = \mathbf{K}_s|_{IJ}^{ab}(\mathbf{U}) = \int_\Omega s_{IJ}(\mathbf{U}) \mathrm{N}^b \mathrm{N}^a \mathrm{d}\Omega, \qquad a, b = 1, \ldots, n_\mathrm{p}$$

where $I, J = 1,\ldots, n_{unk}$.

The source array is given by:

$$\mathbf{F}|^b = \int_\Omega \mathbf{F}\, \mathrm{N}^b \mathrm{d}\Omega, \qquad b = 1, \ldots, n_\mathrm{p}$$

Let us explain how to compute the stabilization term in equation (20). The L^2 projection of the finite element advection term is obtained from the property of projections, which dictates that:

$$\left(\mathbf{V}_h, \mathcal{P}_h\left(\frac{\partial(\boldsymbol{A}_i \boldsymbol{U}_h)}{\partial x_i}\right)\right) = \left(\boldsymbol{V}_h, \frac{\partial(\boldsymbol{A}_i \boldsymbol{U}_h)}{\partial x_i}\right) \qquad \forall \mathbf{V}_h \in \mathcal{V}_h \tag{22}$$

Interpolating

$$\mathcal{P}_h\left(\frac{\partial(\boldsymbol{A}_i \boldsymbol{U}_h)}{\partial x_i}\right) = \sum_{a=1}^{n_\mathrm{p}} \mathbf{R}^a \mathrm{N}^a$$

in equation (22), we obtain block diagonal matrices $\mathbf{M}$ and $\mathbf{L}$ of dimensions $(n_p\ n_{uk} \times n_p\ n_{uk})$, so that the left-hand side can be written as $\mathbf{MR}$ and the right-hand side as $\mathbf{LU}$, where $\mathbf{R}$ is the array with the nodal values of the projection of the convective term. This can now be computed as:

$$\mathbf{MR} = \mathbf{LU}, \qquad \mathbf{R} = \mathbf{M}^{-1}\mathbf{LU} \tag{23}$$

Matrices $\mathbf{M}$ and $\mathbf{L}$ in equation (23) have components:

$$\mathbf{M}|_{IJ}^{ab} = \delta_{IJ} \int_\Omega \mathrm{N}^b \mathrm{N}^a \mathrm{d}\Omega, \qquad a, b = 1, \ldots, n_\mathrm{p}$$
$$\mathbf{L}|_{IJ}^{ab} = \delta_{IJ} \int_\Omega \mathrm{N}^b \left(\boldsymbol{a}_J \cdot \nabla \mathrm{N}\right)^a \mathrm{d}\Omega, \qquad a, b = 1, \ldots, n_\mathrm{p}$$

for all $I, J = 1,\ldots, n_{unk}$.

Using the definitions above, the orthogonal projection is obtained with the following relation:

$$\mathcal{P}_h^{\perp}\left(\frac{\partial(\boldsymbol{A}_i\boldsymbol{U}_h)}{\partial x_i}\right) = \frac{\partial(\boldsymbol{A}_i\boldsymbol{U}_h)}{\partial x_i} - \mathcal{P}_h\left(\frac{\partial(\boldsymbol{A}_i\boldsymbol{U}_h)}{\partial x_i}\right)$$

Let us now introduce the matrices:

$$\mathbf{K}_{\mathrm{oss},1}|_{IJ}^{ab} = \tau_J \delta_{IJ} \int_\Omega \left(\boldsymbol{a}_J \cdot \nabla \mathrm{N}^a\right)\left(\boldsymbol{a}_J \cdot \nabla \mathrm{N}^b\right) \mathrm{d}\Omega, \qquad a,b = 1,\ldots,n_{\mathrm{p}}$$

$$\mathbf{K}_{\mathrm{oss},2}|_{IJ}^{ab} = \tau_J \delta_{IJ} \int_\Omega \left(\boldsymbol{a}_J \cdot \nabla \mathrm{N}^a\right)\mathrm{N}^b \mathrm{d}\Omega, \qquad a,b = 1,\ldots,n_{\mathrm{p}}$$

$$\mathbf{K}_{\mathrm{oss},3}|_{IJ}^{ab} = \tau_J \delta_{IJ} \int_\Omega \mathrm{N}^a \mathrm{N}^b \mathrm{d}\Omega, \qquad a,b = 1,\ldots,n_{\mathrm{p}}$$

where $I, J = 1,\ldots, n_{unk}$. Then, matrix $\mathbf{K}_{\mathrm{oss}}$ arising from the OSS formulation can be written as:

$$\mathbf{K}_{\mathrm{oss}} = \mathbf{K}_{\mathrm{oss},1} - \mathbf{K}_{\mathrm{oss},2}\mathbf{M}^{-1}\mathbf{L} - \mathbf{L}^T\mathbf{M}^{-1}\mathbf{K}_{\mathrm{oss},2}^T + \mathbf{L}^T\mathbf{M}^{-1}\mathbf{K}_{\mathrm{oss},3}\mathbf{M}^{-1}\mathbf{L} \tag{24}$$

3.3 Newton–Raphson linearization

In this section, we perform the linearization of equation (21), whose nonlinearity comes mainly from the reactive term in the applications in which we are interested. To this end, we use Newton–Raphson's algorithm. Let us denote with a subscript counter the iteration level, starting with an initial guess for the unknown $\mathbf{U}_0$. Then, from a given $\mathbf{U}_i$, the next update $\mathbf{U}_{i+1}$ is computed from:

$$\mathbf{U}_{i+1} = \mathbf{U}_i - \mathbf{T}^{-1}(\mathbf{U}_i)\mathbf{r}(\mathbf{U}_i). \tag{25}$$

$\mathbf{T}(\mathbf{U})$ is the tangent stiffness matrix and $\mathbf{r}(\mathbf{U})$ is the residual, defined as follows:

$$\mathbf{r}(\mathbf{U}) = \left(\mathbf{K}_k + \mathbf{K}_a + \mathbf{K}_s(\mathbf{U}) + \mathbf{K}_{\mathrm{oss}}\right)\mathbf{U} - \mathbf{F} \tag{26}$$

$$\mathbf{T}(\mathbf{U}) = \frac{\partial \mathbf{r}(\mathbf{U})}{\partial \mathbf{U}} = \mathbf{K}_k + \mathbf{K}_a + \mathbf{K}_s(\mathbf{U}) + \frac{\partial \mathbf{K}_s(\mathbf{U})}{\partial \mathbf{U}}\mathbf{U} + \mathbf{K}_{\mathrm{oss}} \tag{27}$$

Note that we have exploited the structure of the nonlinearity in the reactive term.

The iterative process is continued until the normalized L^2 norm of the difference between two successive solutions is less than the tolerance. In all cases presented in subsequent sections, the tolerance is set to 10^{-4}.

Another source of nonlinearity arises because of the fact that the stabilization parameters depend on $\boldsymbol{S}$ and therefore they may depend on $\boldsymbol{U}$. We treat this possible nonlinearity using a fixed point scheme, that is to say, if matrix $\boldsymbol{K}_{\mathrm{oss}}$ depends on $\boldsymbol{U}$, the last iterate of this unknown is used for the computation of $\boldsymbol{K}_{\mathrm{oss}}$.

3.4 Time integration

The backward differencing (BDF) scheme is used for the numerical time integration. For a transient nonlinear RDA equation, the total time is split into intervals, where the Newton–Raphson linearization is performed at each interval. Let us denote with a superscript the time step counter and let δt be the time step size of a uniform time step partition. The time discrete version of the transient counterpart of equation (21) using the BDF 1 and BDF 2 schemes is:

$$\left(\frac{\mathbf{M}}{\delta t}+\mathbf{K}_k+\mathbf{K}_a+\mathbf{K}_s(\mathbf{U}^{n+1})+\mathbf{K}_{\text{oss}}\right)\mathbf{U}^{n+1}=\mathbf{F}+\frac{\mathbf{M}}{\delta t}\mathbf{U}^{n} \tag{28}$$

$$\left(\frac{3}{2}\frac{\mathbf{M}}{\delta t}+\mathbf{K}_k+\mathbf{K}_a+\mathbf{K}_s(\mathbf{U}^{n+1})+\mathbf{K}_{\text{oss}}\right)\mathbf{U}^{n+1}=\mathbf{F}+2\frac{\mathbf{M}}{\delta t}\mathbf{U}^{n}-\frac{1}{2}\frac{\mathbf{M}}{\delta t}\mathbf{U}^{n-1} \tag{29}$$

where $\mathbf{M}$ is the mass matrix already introduced in equation (23). The error of equation (28) is first order in time, whereas for equation (29), it is of second order.

When the Newton–Raphson linearization is applied, we obtain additional terms in the definition of the tangent stiffness matrix and the residual with respect to the stationary case. The scheme is initialized taking $\mathbf{U}_0^{n+1}=\mathbf{U}^n$, i.e. the converged solution of the last time step, and then:

$$\mathbf{U}_{i+1}^{n+1}=\mathbf{U}_{i+1}^{n+1}-\mathbf{T}^{-1}\left(\mathbf{U}_i^{n+1}\right)\mathbf{r}\left(\mathbf{U}_i^{n+1}\right) \tag{30}$$

When the BDF 1 scheme is used, we have:

$$\mathbf{r}(\mathbf{U}^{n+1})=\left(\frac{\mathbf{M}}{\delta t}+\mathbf{K}_k+\mathbf{K}_a+\mathbf{K}_s(\mathbf{U}^{n+1})+\mathbf{K}_{\text{oss}}\right)\mathbf{U}^{n+1}-\frac{\mathbf{M}}{\delta t}\mathbf{U}^{n}-\mathbf{F}$$

$$\mathbf{T}(\mathbf{U}^{n+1})=\frac{\mathbf{M}}{\delta t}+\mathbf{K}_k+\mathbf{K}_a+\mathbf{K}_s(\mathbf{U}^{n+1})+\frac{\partial\mathbf{K}_s(\mathbf{U}^{n+1})}{\partial\mathbf{U}}\mathbf{U}^{n+1}+\mathbf{K}_{\text{oss}}$$

and using BDF 2, we have:

$$\mathbf{r}(\mathbf{U}^{n+1})=\left(\frac{3}{2}\frac{\mathbf{M}}{\delta t}+\mathbf{K}_k+\mathbf{K}_a+\mathbf{K}_s(\mathbf{U}^{n+1})+\mathbf{K}_{\text{oss}}\right)\mathbf{U}^{n+1}-2\frac{\mathbf{M}}{\delta t}\mathbf{U}^{n}$$
$$+\frac{1}{2}\frac{\mathbf{M}}{\delta t}\mathbf{U}^{n-1}-\mathbf{F}$$

$$\mathbf{T}(\mathbf{U}^{n+1})=\frac{3}{2}\frac{\mathbf{M}}{\delta t}+\mathbf{K}_k+\mathbf{K}_a+\mathbf{K}_s(\mathbf{U}^{n+1})+\frac{\partial\mathbf{K}_s(\mathbf{U}^{n+1})}{\partial\mathbf{U}}\mathbf{U}^{n+1}+\mathbf{K}_{\text{oss}}$$

This scheme needs to be initialized with BDF 1 for $n=0$.

4. Numerical tests

A study to demonstrate the optimal convergence rates found with the numerical formulation proposed has been carried out using the method of manufactured solutions. An analytical solution that satisfies the initial and boundary conditions was chosen and the source term in the RDA equation was modified so that the chosen solution satisfies the RDA equation. The

numerical solution was then compared against the analytical one for each of the following cases:

- stationary nonlinear RDA equation;
- transient nonlinear RDA equation; and
- transient nonlinear system of coupled RDA equations.

Tests were conducted for different values of the coefficients. The advection velocity used is given by $\boldsymbol{a} = |\mathbf{a}|\left(\cos\left(\frac{\pi}{3}\right), \sin\left(\frac{\pi}{3}\right)\right)^T$, where $|\mathbf{a}|$ is a norm of the velocity. The direction of the velocity field was chosen so that it did not align with the mesh, which consisted of linear quadrilateral elements along coordinate axes. The non-dimensional numbers were based on the uniform mesh in the domain and not on local mesh refinements carried out in regions of sharp layers. Such local refinements were carried out only to mitigate the presence of oscillatory solution in the region of these sharp gradients.

4.1 Stationary nonlinear reaction–diffusion–advection equation

Consider the Fischer–KPP equation with logistic growth term, given by:

$$\begin{aligned} -k\Delta u + \boldsymbol{a}\cdot\nabla u - su(1-u) &= f \quad \text{in } \Omega = [0,1]\times[0,1] \\ u &= 0 \quad \text{on } \partial\Omega \end{aligned} \tag{31}$$

The stabilization parameter in this case was chosen as:

$$\tau^{-1} = \frac{4k}{h^2} + \frac{2|\boldsymbol{a}|}{h} + s(1-\max(u)) \tag{32}$$

where $\max(u)$ is the maximum of the unknown u in Ω. As τ depends on u, it has to be computed iteratively, with $\max(u)$ computed with the last iterate of u.

The convergence tests were carried out for various values of coefficients, as shown in Table I. Pe and Da numbers based on the finest mesh are indicated. The normalized L^2 norm of the error is a function of the mesh size. Let $\tilde{u}_h$ be the piecewise linear finite element interpolation of u; then the L^2 norm of the error can be bounded by:

$$||u - \tilde{u}_h||_{L^2} \leq Ch^2||D^2u||_{L^2}$$

where C is a constant and D^2u is the Hessian of u. Thus, for linear finite element interpolation, the L^2 error is of order $O(h^2)$. Hence, the convergence in space plot in log-log scale must yield a slope of 2 if the finite element error is optimal. Figure 1 shows indeed optimal convergence rates with various test cases for two examples with analytical solution, given by:

ID	k	$\lvert\mathbf{a}\rvert$	s	h	Pe	Da
Test1	1.00E-04	1.00E-04	1.00E-04	2.00E-02	1.00E-02	4.00E-04
Test2	1.00E-04	1.00E-04	1.00E 01	2.00E-02	1.00E-02	4.00E 01
Test3	1.00E-04	1.00E 00	1.00E-04	2.00E-02	1.00E 02	4.00E-04
Test4	1.00E-04	1.00E 00	1.00E 01	2.00E-02	1.00E 02	4.00E 01

Table I. Tests for stationary nonlinear RDA equation

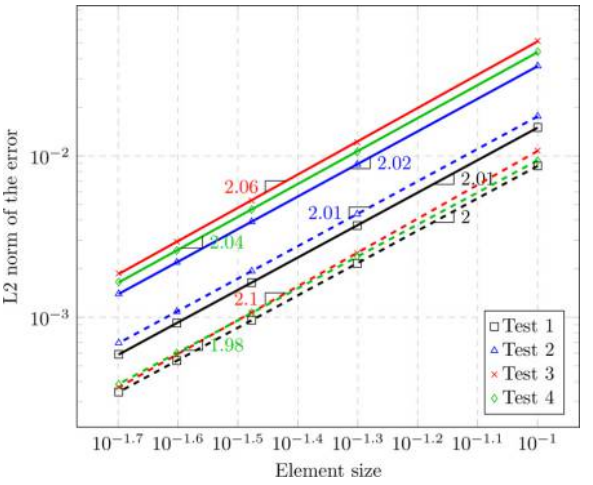

Figure 1.
Convergence plot for stationary nonlinear RDA equation for Example 1 (solid) and Example 2 (dashed)

$$\text{Example 1}: u = x^2(1-x^2)y^2(1-y^2)$$
$$\text{Example 2}: u = x(1-x)y(1-y)$$

This example serves to show that the stabilization terms introduced yield optimal convergence when the solution is smooth when the physical parameters have very different scales.

4.2 Transient nonlinear reaction–diffusion–advection equation

The transient Fischer–KPP equation with initial and boundary conditions as shown below was considered for convergence tests:

$$\begin{aligned} &\frac{\partial u}{\partial t} - k\Delta u + \boldsymbol{a}\cdot\nabla u - su(1-u) = f \quad \text{in } \Omega = [0,1]\times[0,1], t > 0 \\ &u = 0 \quad \text{in } \Omega, t = 0 \\ &u = 0 \quad \text{on } \partial\Omega, t > 0 \end{aligned} \tag{33}$$

The same expression [equation (32)] as in the previous example was used for the stabilization parameter, now with u evaluated in the previous iteration of the current time step of the temporal discretization.

The time interval under consideration was [0, 1]. BDF 2 time integration scheme was used. The solution error in the L^2 norm at the end of time interval was measured for various time step sizes. Figure 2 shows the convergence plot for different test cases in Table II for two examples whose analytical solutions are given by:

$$\text{Example 1}: u = 2t^3x(1-x)y(1-y)$$
$$\text{Example 2}: u = \sin\left(\frac{\pi t}{2}\right)x(1-x)y(1-y)$$

For characteristic mesh size h and time step size δt, the optimal behavior of the error in the L^2 norm to be expected is given by the estimate:

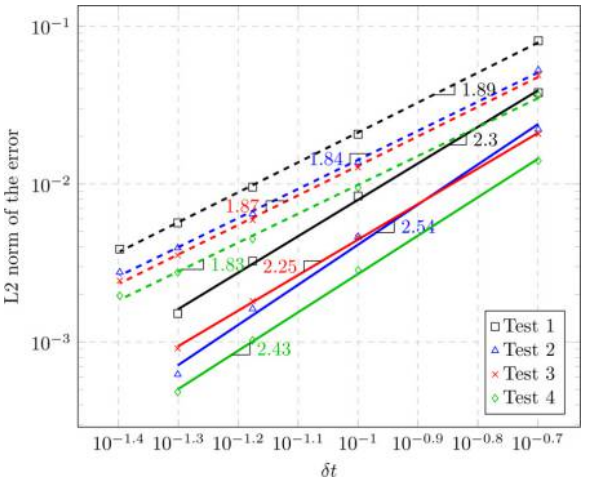

Figure 2.
Convergence plot for transient nonlinear RDA equation for Example 1 (solid) and Example 2 (dashed)

ID	k	$\|\mathbf{a}\|$	s	h	Pe	Da
Test1	1.00E-04	1.00E-04	1.00E-04	1.25E-02	6.25E-03	1.56E-04
Test2	1.00E-04	1.00E-04	1.00E 01	1.25E-02	6.25E-03	1.56E 01
Test3	1.00E-04	1.00E 00	1.00E-04	1.25E-02	6.25E 01	1.56E-04
Test4	1.00E-04	1.00E 00	1.00E 01	1.25E-02	6.25E 01	1.56E 01

Table II.
Tests for transient nonlinear RDA equation

$$\sqrt{\sum_n \delta t ||u(t^n) - u_h^n||_{L^2}^2} \leq C_1 h^2 \max_t ||D^2 u|| + C_2 \delta t^2 \max_t \left\| \frac{\partial^2 u}{\partial t^2} \right\|_{L^2}$$

where summation extends to all time steps of the partition in time, u(t^n) is the exact solution evaluated at $t^n = n\delta t$ and C_1 and C_2 are constants. Neglecting the error due to spatial discretization by considering a fine mesh the dependency of error on time is $O(\delta t^2)$. Therefore for the convergence plot of the normalized error measured in the L^2 norm, we anticipate a slope of 2 in log-log scale. This is what we have found, and what is shown in Figure 2.

4.3 Transient nonlinear system of coupled reaction–diffusion–advection equations

A system of transient RDA equations coupled through the nonlinear reaction term was also considered. The nonlinearity in reaction is of the logistic form for both equations. The problem reads: find u_1 and u_2 such that:

$$\begin{bmatrix} \frac{\partial u_1}{\partial t} \\ \frac{\partial u_2}{\partial t} \end{bmatrix} - \begin{bmatrix} k_1 \Delta u_1 \\ k_2 \Delta u_2 \end{bmatrix} + \begin{bmatrix} \boldsymbol{a}_1 \cdot \nabla u_1 \\ \boldsymbol{a}_2 \cdot \nabla u_2 \end{bmatrix} \tag{34}$$

$$-\begin{bmatrix} s_{11}u_1(1-u_1) & s_{12}u_1(1-u_2) \\ s_{21}u_2(1-u_1) & s_{22}u_2(1-u_2) \end{bmatrix} = \begin{bmatrix} f_1 \\ f_2 \end{bmatrix} \quad \text{in } \Omega = [0,1]\times[0,1], t > 0$$
$$u_1 = u_2 = 0 \quad \text{in } \Omega, t = 0$$
$$u_1 = u_2 = 0 \quad \text{on } \partial\Omega, t > 0 \tag{35}$$

The matrix of stabilization parameters used for this problem is $\tau = \text{diag}\,(\tau_1, \tau_2)$, where:

$$\tau_1^{-1} = \frac{4k_1}{h^2} + \frac{2|\boldsymbol{a}_1|}{h} + s_{11}\left(1 - \max(u_1)\right) + s_{12}\left(1 - \max(u_2)\right)$$
$$\tau_2^{-1} = \frac{4k_2}{h^2} + \frac{2|\boldsymbol{a}_2|}{h} + s_{21}\left(1 - \max(u_1)\right) + s_{22}\left(1 - \max(u_2)\right)$$

with the unknowns u_1 and u_2 evaluated at the previous iteration of the current time step.

Newton–Raphson iterations were performed until the respective differences between successive solutions of both u_1 and u_2 were below the specified tolerance. The analytical solution of this example was taken as:

$$u_1 = t^2 x(1-x)y(1-y)$$
$$u_2 = \sin\left(\frac{\pi t}{2}\right) x(1-x)y(1-y)$$

The same comments concerning optimal convergence as for the scalar equation of the previous example apply in the present case. Figure 3 shows optimal convergence in time for u_1 and u_2 for the different tests shown in Table III.

5. Applications

The application of the OSS scheme for the finite element approximation of a nonlinear RDA equation in the lid-driven cavity flow and for a predator-prey model consisting of a system of transient nonlinear–coupled RDA equations is now presented. Attention is drawn to the stability of the solution scheme for high Pe and Da numbers. Also the ability of the formulation to capture sharp layers in the solution with selective mesh refinement is highlighted.

A homogeneous initial condition results in a system that remains homogeneous throughout the evolution of time, without the formation of spatial patterns (Medvinsky *et al.*, 2002). Non-homogeneous initial conditions are therefore considered. In all cases, SI units have been assumed.

5.1 Cavity flow

The lid-driven cavity flow is a fluid flow problem in a square domain with three stationary walls and one moving boundary (usually the top) whose velocity field is obtained by solving the incompressible Navier–Stokes equation. The velocity field generated is dependent on the Reynolds number, which is defined as $\text{Re} = ULv^{-1}$, where U is a characteristic velocity, L a characteristic (global) length and ν the kinematic viscosity of the fluid. In this problem, we take $L = 1$ and $U = 1$, the velocity on the lid of the cavity. Generally, a steady field is obtained up to a Reynolds number below 10^4, after which the solution is transient. Hence, steady state velocity fields for Re = 200 and 4,000, shown in Figure 4, were used for the tests, as they represent distinct features in their vortical structures.

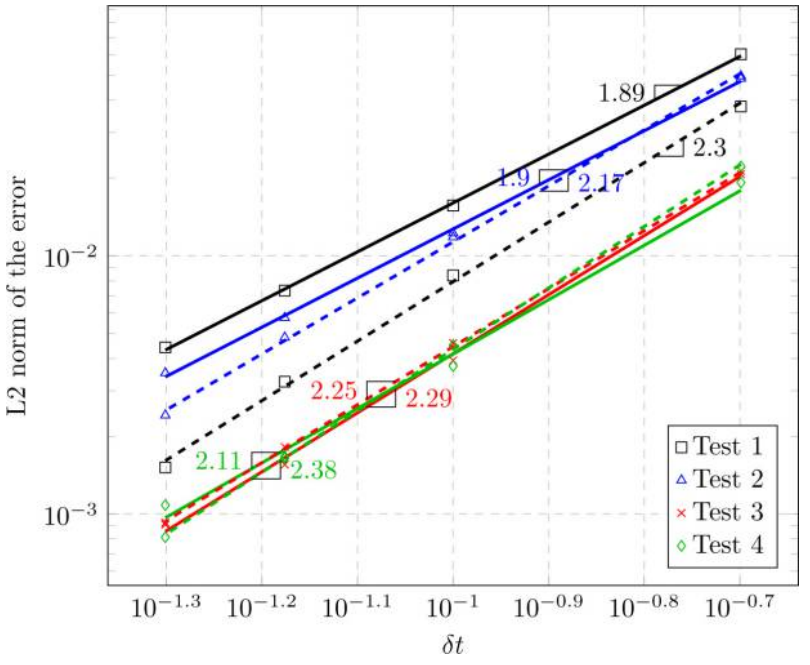

Figure 3.
Convergence plot for transient nonlinear system of coupled RDA equations for u_1 (solid) and u_2 (dashed)

ID	k_1, k_2	a	s_{11},s_{12},s_{21},s_{22}	h	Pe	Da
Test1	1.00E-04	1.00E-04	1.00E-04	2.00E-02	1.00E-02	4.00E-04
Test2	1.00E-04	1.00E-04	1.00E 01	2.00E-02	1.00E-02	4.00E 01
Test3	1.00E-04	1.00E 00	1.00E-04	2.00E-02	1.00E 02	1.00E-04
Test4	1.00E-04	1.00E 00	1.00E 01	2.00E-02	1.00E 02	4.00E 01

Table III.
Tests for transient nonlinear system of coupled RDA equations

The transient, nonlinear RDA equation of Fisher–KPP kind was solved in the domain with the advection field of the cavity flow problem. This flow generates a large central eddy and smaller eddies along the corners depending on Re. Such velocity fields pose challenges in obtaining numerical solution to the RDA equation. The objective is to demonstrate the capability of the OSS finite element method in providing smooth solutions to RDA equation with high Pe and Da numbers in a complex flow field.

The time evolution of the distribution of species is the solution sought. In the present case, diffusion is weak, with value $k = 10^{-4}$, and reaction is strong, with $s = 1$. The maximum velocity on the top surface has unit magnitude, as shown in Figure 4. The problem is stated as follows: find u such that:

$$\frac{\partial u}{\partial t} - k\Delta u + \boldsymbol{a} \cdot \nabla u + su(1-u) = f \quad \text{in } \Omega = [0\ 1] \times [0\ 1],\ t > 0 \tag{36}$$

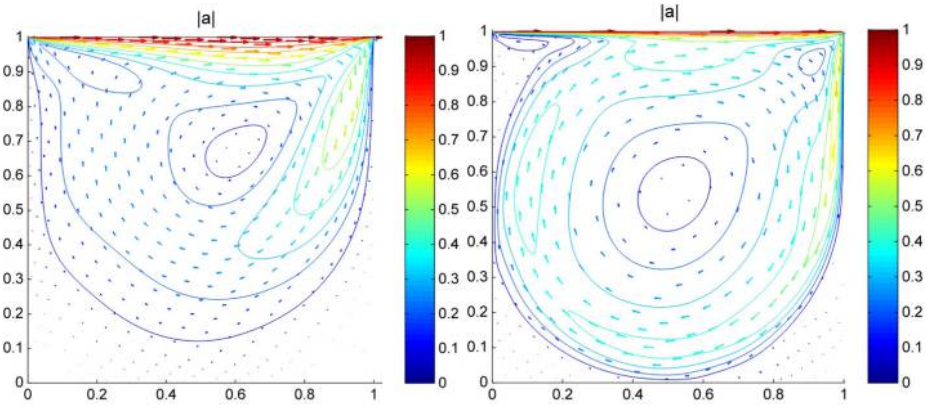

Figure 4.
Cavity flow velocity field for test cases

Notes: Left: Re = 200, right: Re = 4,000

$$u(x=0,y,t)=u(x=1,y,t)=u(x,y=0,t)=0$$
$$u(x,y,t=0)=\begin{cases}10(y-0.9), & y>0.9\\ 0, & \text{elsewhere}\end{cases} \tag{37}$$

where $\boldsymbol{a}$ is the velocity field shown in Figure 4. The boundary condition at $y = 1$ is zero flux, i.e. $\partial u/\partial y = 0$ at $y = 1$. At the discrete level, this boundary condition is also applied at the corners (0, 1) and (1, 1).

The problem consists of large convection and reaction processes relative to diffusion. Sharp layers in the solution were anticipated and hence careful considerations for mesh size and selective refinement were made. The problem was initially solved with a coarse mesh to determine the distribution of u. For Re = 200, u was found to get transported in the whole domain; hence an overall fine mesh of size $h = 1/75$ was chosen with 0.1 units wide zone of refinement of mesh size 1/150 along the boundaries. For Re = 4,000, u was found to evolve being transported close to the domain boundaries. Hence, an overall coarse mesh of size $h = 1/50$, with 0.2 units wide zone of refinement of mesh size 1/100 near the boundaries was found to be a good choice. Pe and Da were determined on the basis of overall mesh size. Note that Pe was based on the velocity at the top of the cavity. Thus for the problem with Re = 200, Pe = 67 and Da = 1.8, and for Re = 4,000, Pe = 100 and Da = 4.

Snapshots at different times of the solution for Re = 200 are shown in Figure 5. Dominant advection and reaction phenomena are observed to be driving the process. Also the effect of a finer mesh in increasing the resolution of the solution is depicted clearly in the figures corresponding to $t = 2$, $t = 2.5$ and $t = 3$, in which sharp layers are observed close to the right boundary. In the solution for Re = 4,000 shown in Figure 6, one can observe that the evolution of species caught up in small eddies in this flow regime is well captured.

5.2 Predator–prey system

As an example of coupled system of nonlinear equations, we consider a predator–prey model in ecological interactions, with time-continuous properties, describing population dynamics in terms of a spatially and temporally continuous density function.

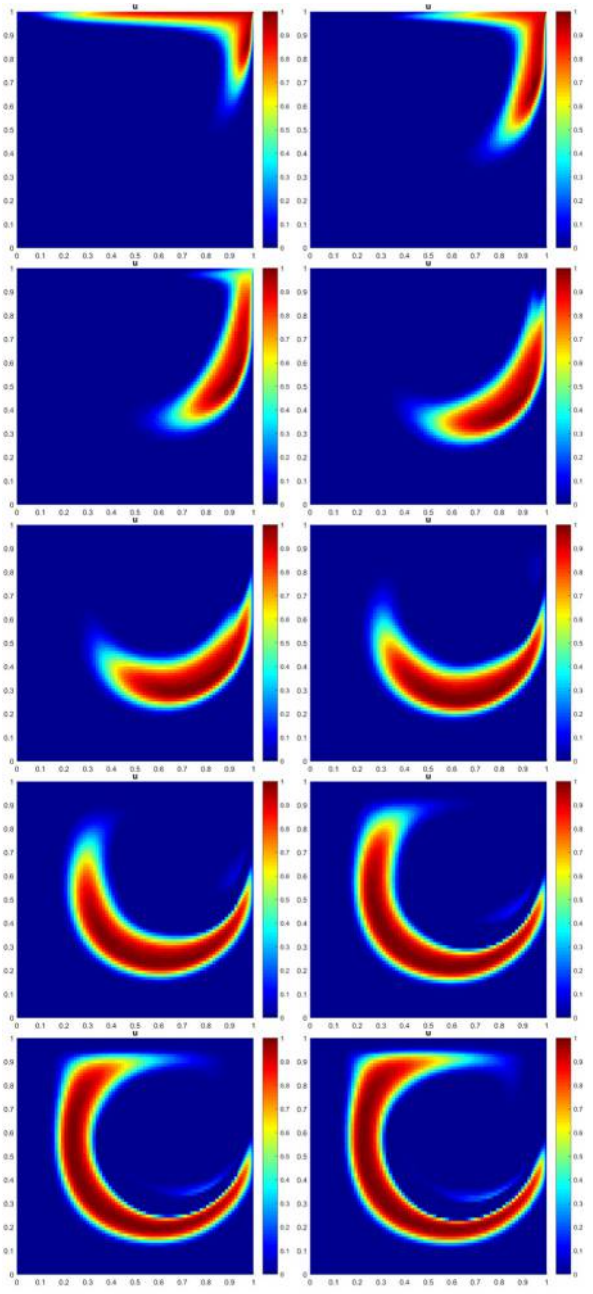

Notes: From the left to the right and from the top to the bottom: $t = 0.5, 1, 1.5, 2, 2.5, 3, 3.5, 4, 4.5, 5$

Figure 5.
Snapshot of RDA solution u for Re = 200, Pe = 67 and Da = 1.8

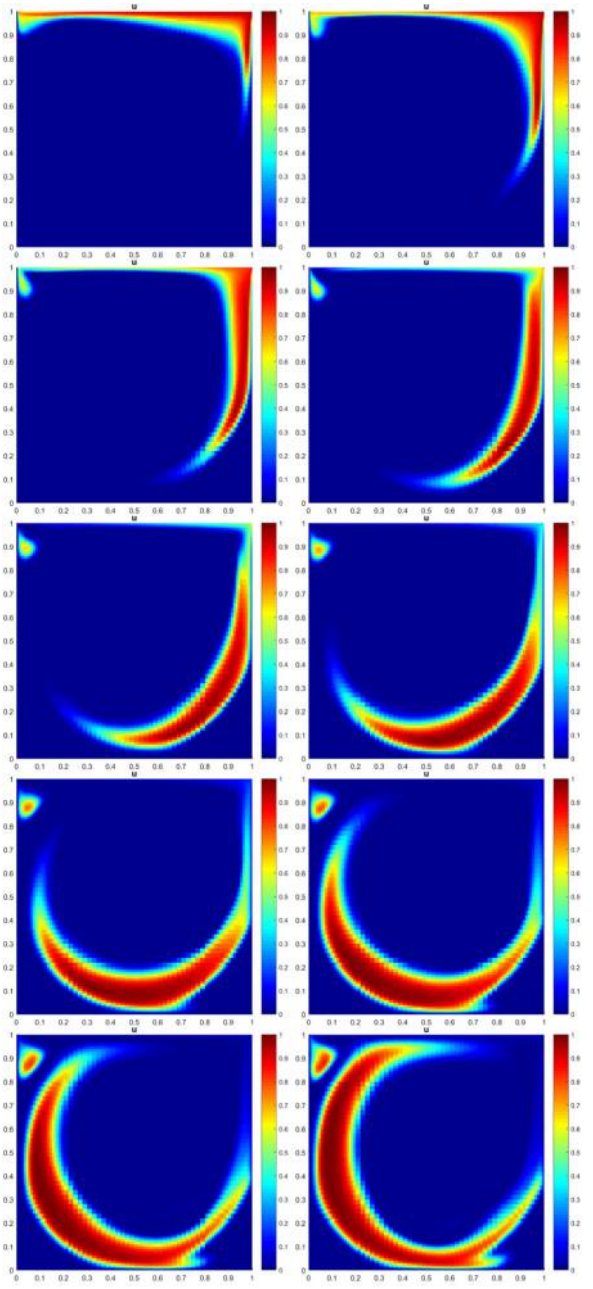

Notes: From the left to the right and from the top to the bottom: $t = 0.5, 1, 1.5, 2, 2.5, 3, 3.5, 4, 4.5, 5$

Figure 6.
Snapshot of RDA solution u for Re = 4,000, Pe = 100 and Da = 4

When population studies were required to be initiated, it was found that species-specific studies were discouragingly complicated for a system with large number of interacting entities. The easiest simplification was to reduce the complexity to just the interaction between two "functional groups," zooplanktons and photoplanktons. This binary description worked good in empirical sense too. The next step was to formulate the model and discover properties such as existence, stability and bounds of the solution, periodicity or pattern formation and bifurcation. It was not the intention of the present study to delve in these aspects. Rather, when such system is required to be solved for different values of parameters of the equations, addressing the challenges encountered in obtaining a numerical solution when the scales of these parameters are hugely different was the main intention.

In the next section, we briefly describe the origin of the predator–prey model used in the present work. Much of the details about the model can be obtained in Malchow's (2008) book.

5.2.1 Formulation of predator–prey model. A generalized starting point for a closed system predator–prey model is the transient diffusion–reaction equation. The general form is as follows:

$$\frac{\partial u_1}{\partial t} = k_1 \Delta u_1 + P(u_1) - E(u_1, u_2)$$
$$\frac{\partial u_2}{\partial t} = k_2 \Delta u_2 + \kappa E(u_1, u_2) - \mu(u_2)$$

where u_1 and u_2 represent the population densities of the prey and predator, respectively. $P(u_1)$ is the prey population growth function. $E(u_1, u_2)$ represents the act of predation, resulting in a decline of prey and growth of predator populations. κ is the predation efficiency which determines the effectiveness of predation on the growth of predator population. $\mu(u_2)$ quantifies predator mortality. Hence, the prey equation consists of terms for spreading of prey population, growth by reproduction P and demise by predation E. On the other hand, the predator equation consists of terms for its spreading, growth by predation E (with κ efficiency, where $0 \leq \kappa \leq 1$) and death by mortality μ.

One of the popular approaches to model functions P, E and μ is:

$$\frac{\partial u_1}{\partial t} = k_1 \Delta u_1 + C u_1 \left(1 - \frac{u_1}{K}\right) - B \frac{u_1 u_2}{u_1 + H}$$
$$\frac{\partial u_2}{\partial t} = k_2 \Delta u_2 + \kappa B \frac{u_1 u_2}{u_1 + H} - M u_2$$

where the predator functional response to the prey density E is modeled by the so-called Hollinger type II model, B represents the predation rate and the parameter H has the meaning of the half-saturation prey density. To model prey population growth, a logistic term is used. C represents the prey growth rate and K is the carrying capacity of the system, which denotes the maximum population of prey supported by the domain, assumed to be unity in our tests. Also, the predator mortality μ is given by a linear term, M being its coefficient.

Adding to this, a seasonal migration pattern or migrations towards regions of resource availability can be introduced via an advection term. This models the bulk movement of populations. Thus the final predator-prey system to be considered is obtained, which may be solved with suitable initial and boundary conditions. This system is:

$$\begin{bmatrix} \frac{\partial u_1}{\partial t} \\ \frac{\partial u_2}{\partial t} \end{bmatrix} - \begin{bmatrix} k_1 \Delta u_1 \\ k_2 \Delta u_2 \end{bmatrix} + \begin{bmatrix} \boldsymbol{a}_1 \cdot \nabla u_1 \\ \boldsymbol{a}_2 \cdot \nabla u_2 \end{bmatrix} - \begin{bmatrix} s_{11}(1-u_1) & -s_{12}\frac{u_1}{1+\alpha_1 u_1} \\ -s_{21}\frac{u_2}{1+\alpha_2 u_1} & s_{22} \end{bmatrix} \begin{bmatrix} u_1 \\ u_2 \end{bmatrix} = \begin{bmatrix} 0 \\ 0 \end{bmatrix}$$

In these equations, $s_{11} = C$, $K = 1$, $s_{12} = \frac{B}{H}$, $\alpha_1 = \frac{1}{H}$, $s_{21} = \frac{\kappa B}{H}$, $\alpha_2 = \frac{1}{H}$ and $s_{22} = -M$. The advection velocity for the prey is $\boldsymbol{a}_1$ and for the predator $\boldsymbol{a}_2$. Note that the (nonlinear) coupling of equations occurs in their respective reaction terms.

5.2.2 Numerical tests and results. Let us consider the predator–prey equation within a unit square domain with zero Dirichlet boundary conditions and initial condition (population densities of predator and prey), as shown in Figure 7.

A number of cases were run for different values of the reaction coefficients s_{11}, s_{12}, s_{21} and s_{22}, indicated in Table IV. The rest of physical coefficients were retained as constant for all the cases. In particular, the diffusion coefficients was taken as $k_1 = k_2 = 10^{-4}$ and the advection velocity fields were $\boldsymbol{a}_1 = 0.5(1,1)^T$ and $\boldsymbol{a}_1 = 0.5(-1,-1)^T$. In this case, predator and prey populations are driven in opposite directions for head-on encounter with one another. No source terms were considered and the constants α_1 and α_2 were taken to be unity. The system of equations of the model reads:

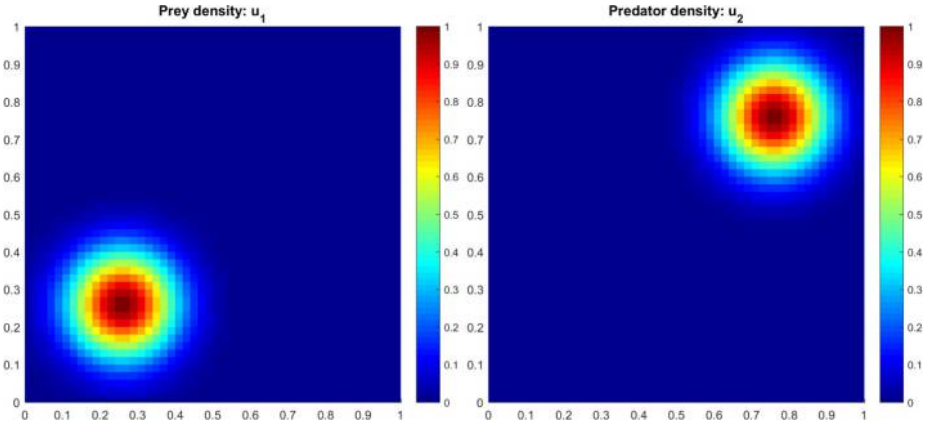

Figure 7.
Predator-prey initial condition for all test cases

ID	s_{11}	s_{12}	s_{21}	s_{22}
Case 1	0	0	0	0
Case 2	0	0	0	1
Case 3	0	0	3	1
Case 4	1	0	3	1
Case 5	1	2	3	1

Table IV.
Predator–prey test cases for different reaction coefficients

$$\begin{bmatrix} \frac{\partial u_1}{\partial t} \\ \frac{\partial u_2}{\partial t} \end{bmatrix} - 10^{-4} \begin{bmatrix} \Delta u_1 \\ \Delta u_2 \end{bmatrix} + 0.5 \begin{bmatrix} \frac{\partial u_1}{\partial x_1} + \frac{\partial u_1}{\partial x_2} \\ \frac{\partial u_2}{\partial x_1} + \frac{\partial u_2}{\partial x_2} \end{bmatrix} - \begin{bmatrix} s_{11}(1-u_1) & -s_{12}\frac{u_1}{1+u_1} \\ -s_{21}\frac{u_1}{1+u_1} & s_{22} \end{bmatrix} \begin{bmatrix} u_1 \\ u_2 \end{bmatrix} = \begin{bmatrix} 0 \\ 0 \end{bmatrix}$$

to be solved in the domain $\Omega = [0,1] \times [0,1]$ where the initial population densities are normal distributions as shown below:

$$u_1(x, y, t = 0) = e^{-50\left((x-0.25)^2+(y-0.25)^2\right)} \tag{38}$$

$$u_2(x, y, t = 0) = e^{-50\left((x-0.75)^2+(y-0.75)^2\right)}. \tag{39}$$

The domain was discretized with quadrilateral elements with element size $h = 0.02$. Hence, Pe = 50, and considering the maximum values of s_{11} and s_{22}, Da = 4. The temporal domain was [0,1]. Solution snapshots at $t = 0.2, 0.4, 0.6, 0.8, 1$ are presented for each case that was run.

Case 1 represents the absence of reaction terms. Diffusion is relatively weak compared to advection. The equations are uncoupled and independent of each other. In Figure 8, we can observe a small diffusion and consequently large advection of the population along the direction of the advection velocity. As there is no interaction, the populations of predator and prey do not affect each other. This case is important to observe the effect of transport and diffusion alone. It will serve as a reference for comparison to cases with reaction terms.

In Case 2, $s_{22} = 1$. The prey population is still governed by advection–diffusion but the predator is governed by an RDA equation with linear reaction. The linear reaction term models the decline of the predator because of lack of availability of prey. Hence, we expect a temporal decline of population of predator and we can observe that in Figure 9. As in Case 1, both equations are uncoupled and independent of one another. Hence the solution for the prey remains the same as in Case 1.

Case 3 adds more complexity to the predator equation with $s_{22} = 1$ and $s_{21} = 3$. For the predator, the contribution of decline of species by mortality and growth by predation is added. We can see that it is now linked to the prey population through a one-way coupling (prey population is not affected by predator). This is evident in Figure 10. In the first two time instants shown, the predator population declines, but after encountering the prey, the predator population rapidly increases, as depicted in the snapshots for $t = 0.6$ and $t = 0.8$. At $t = 1$, we observe that predator population declines again in the absence of prey.

Case 4 introduces a logistic growth reaction term for the prey population. In this case, along with $s_{22} = 1$ and $s_{21} = 3$, we also have $s_{11} = 1$. We can expect to observe growth in population of prey. But the equations are just one-way coupled. The growth of prey population is indicated in Figure 11. Due to altered prey population, the dynamics of predator is different too.

Case 5 is the most realistic and comprehensive case. Growth and decline of populations of both prey and predator are considered and there is a two-way coupling in the system of equations. The prey population grows in a logistical manner with mortality by predation. On the other hand, predation fuels the growth of predator, but its mortality controls overpopulation. Predation occurs when both populations meet spatially at the same time. The behavior is highly nonlinear as seen in Figure 12. Diffusion, advection and reaction terms compete to produce a net result, in which species populations interact between them.

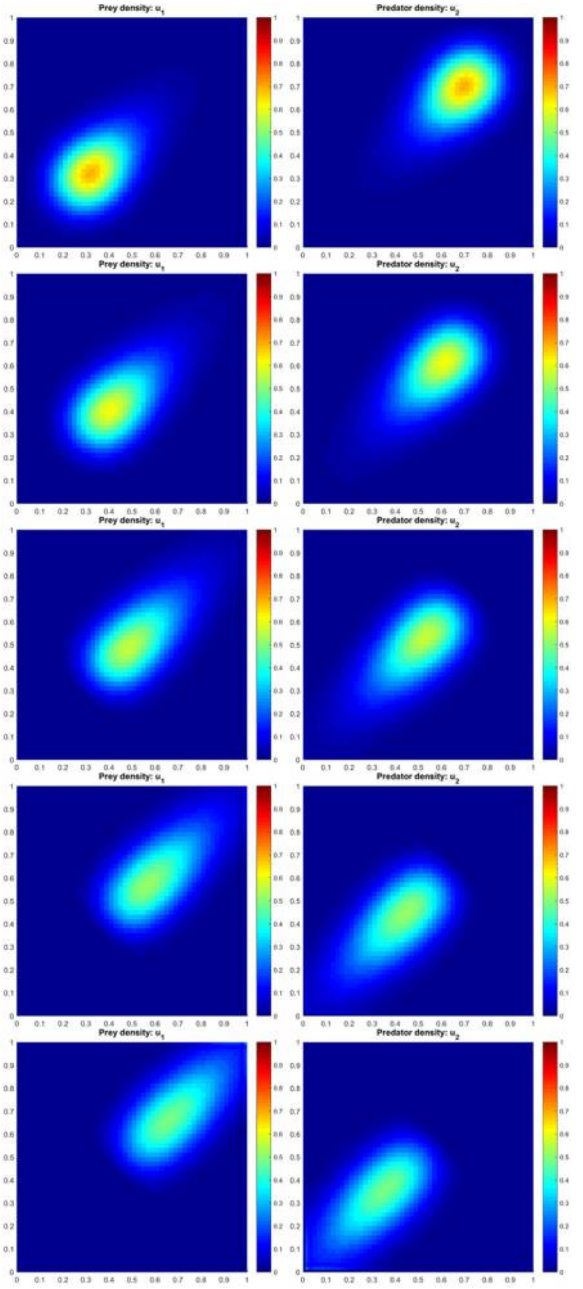

Notes: From the top to the bottom: $t = 0.2$, 0.4, 0.6, 0.8, 1.0; left: prey concentration; right: predator concentration

Figure 8.
Predator-prey densities for Case 1 in Table IV

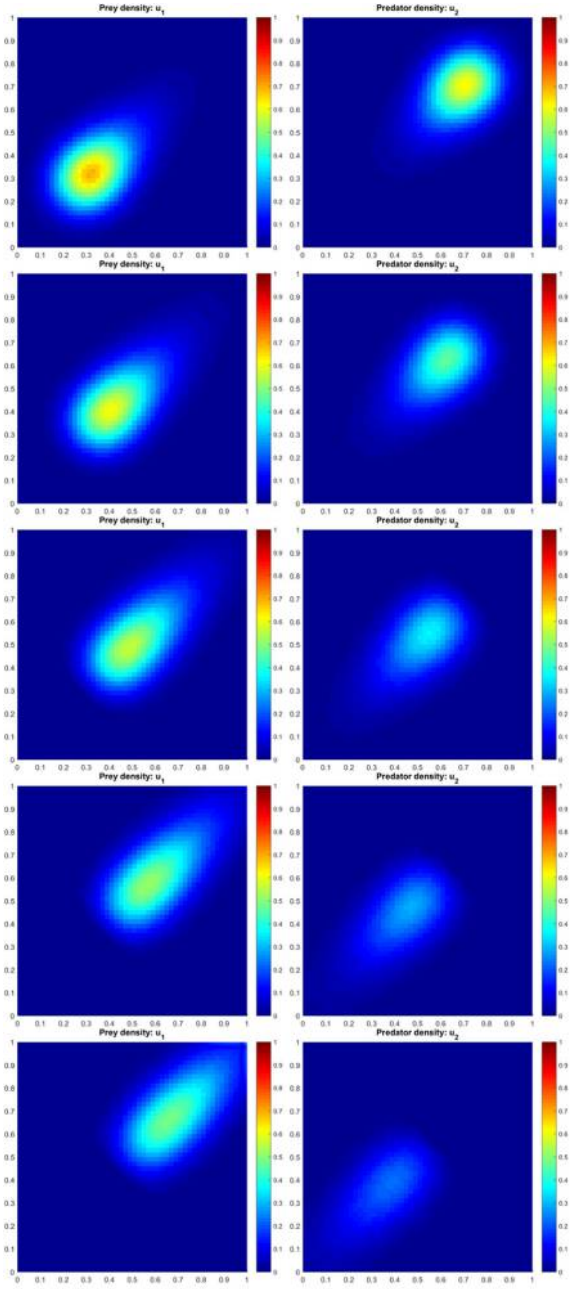

Notes: From the top to the bottom: $t = 0.2, 0.4, 0.6, 0.8, 1.0$; left: prey concentration; right: predator concentration

Figure 9.
Predator-prey densities for Case 2 in Table IV

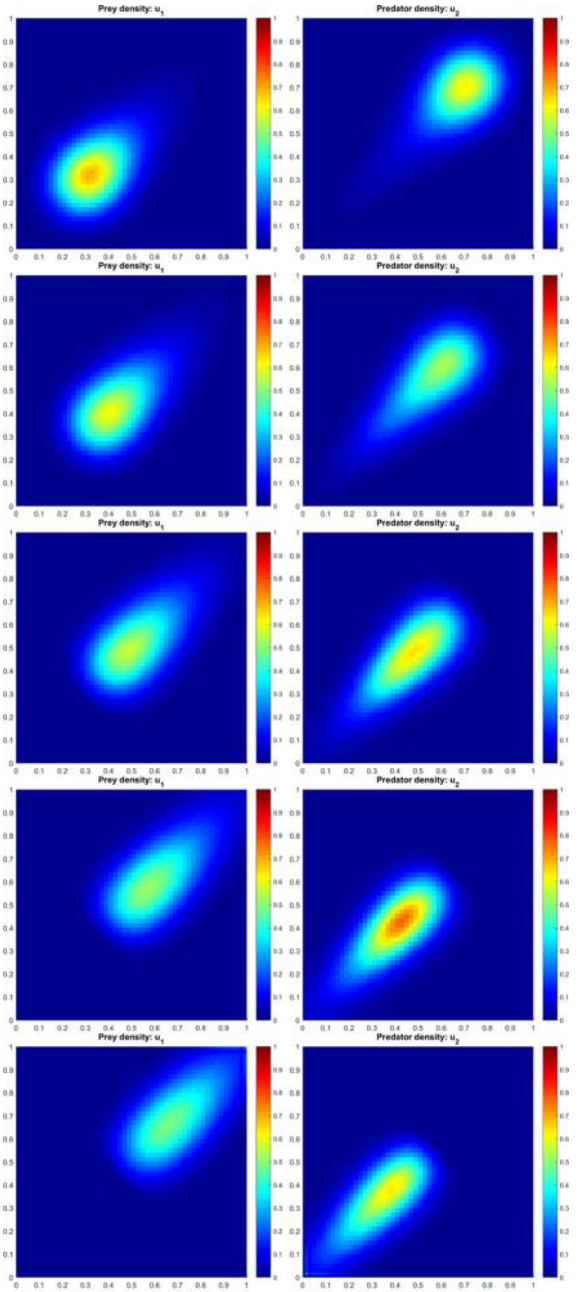

Notes: From the top to the bottom: $t = 0.2, 0.4, 0.6, 0.8, 1.0$; left: prey concentration; right: predator concentration

Figure 10.
Predator-prey densities for Case 3 in Table IV

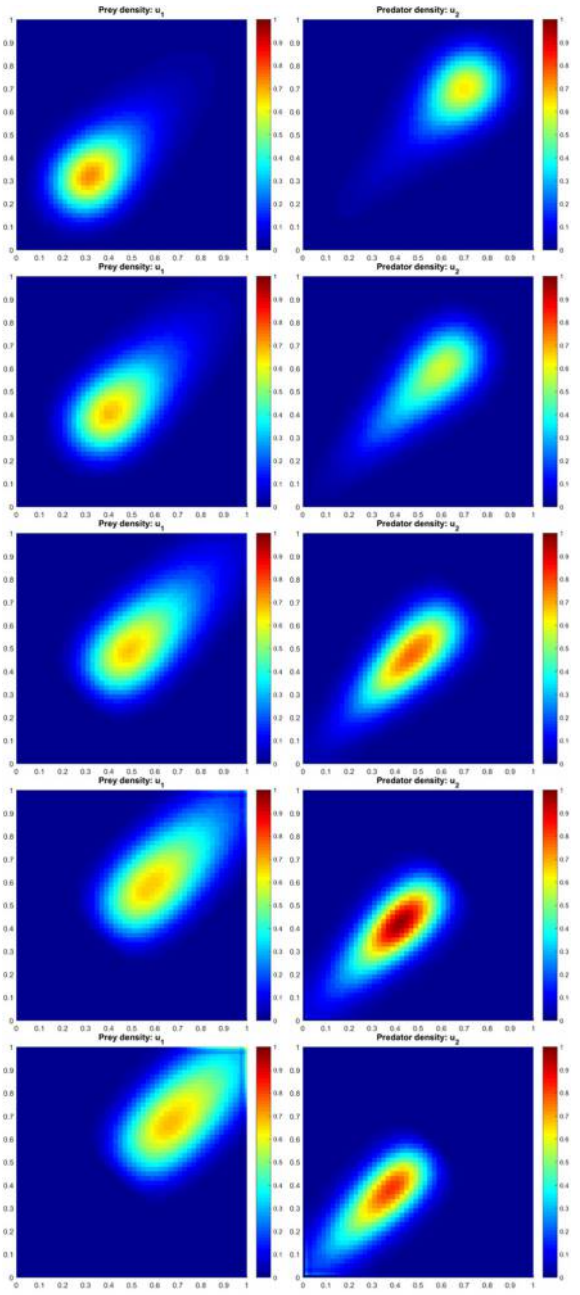

Notes: From the top to the bottom: $t = 0.2$, 0.4, 0.6, 0.8, 1.0; left: prey concentration; right: predator concentration

Figure 11.
Predator-prey densities for Case 4 in Table IV

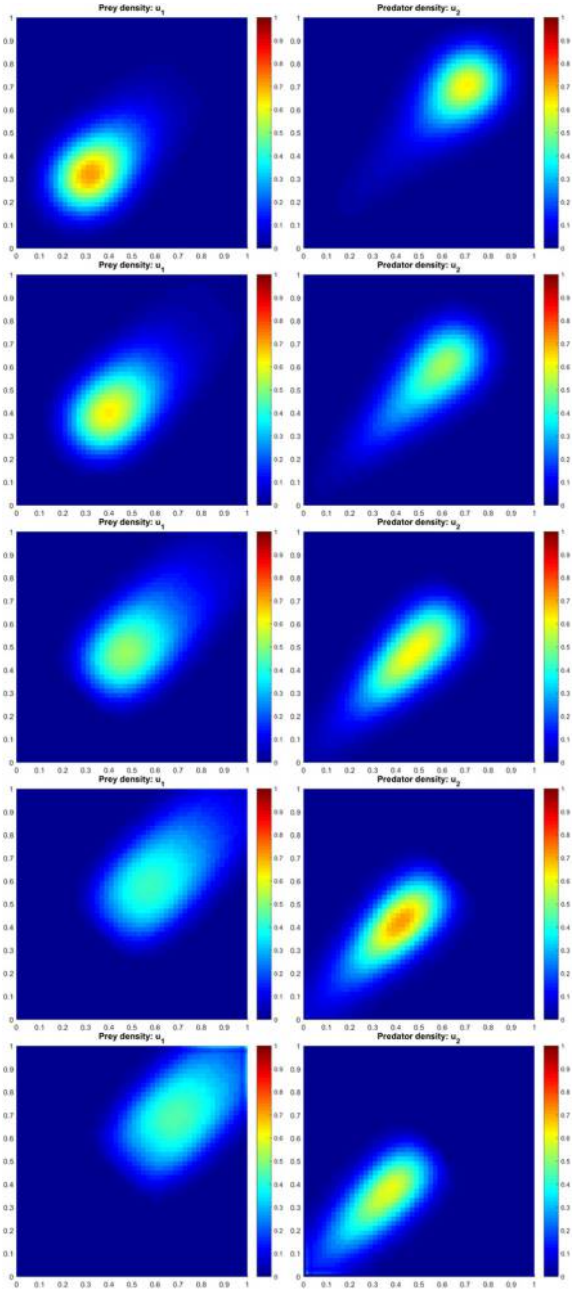

Notes: From the top to the bottom: t = 0.2, 0.4, 0.6, 0.8, 1.0; left: prey concentration; right: predator concentration

Figure 12.
Predator-prey densities for Case 5 in Table IV

6. Conclusions

In this paper, we have presented a numerical model to approximate systems of nonlinear RDA equations. The main ingredients are a stabilized finite element discretization for the space discretization, temporal integration using finite differences and an appropriate linearization of the nonlinear reactive terms. The finite element method proposed is the most significant contribution. In the numerical examples presented, we have shown that it provides optimal accuracy, both in space and in time, when combined with the BDF 2 time integration. We have also presented two application examples in which the robustness of the method has been demonstrated. We have shown that it is able to deal with cases in which diffusion is small and the physics of the problem is governed by nonlinear reaction, convection or both.

References

Codina, R. (1998), "Comparison of some finite element methods for solving the diffusion-convection-reaction equation", *Computer Methods in Applied Mechanics and Engineering*, Vol. 156 Nos 1-4, pp. 185-210.

Codina, R. (2000), "On stabilized finite element methods for linear systems of convection diffusion-reaction equations", *Computer Methods in Applied Mechanics and Engineering*, Vol. 188 Nos 1-3, pp. 61-82.

Codina, R. (2002), "Stabilized finite element approximation of transient incompressible flows using orthogonal subscales", *Computer Methods in Applied Mechanics and Engineering*, Vol. 191 Nos 39/40, pp. 4295-4321.

Codina, R. and Blasco, J. (2002), "Analysis of a stabilized finite element approximation of the transient convection-diffusion-reaction equation using orthogonal subscales", *Computing and Visualization in Science*, Vol. 4 No. 3, pp. 167-174.

Codina, R., Principe, J. and Baiges, J. (2009), "Subscales on the element boundaries in the variational two-scale finite element method", *Computer Methods in Applied Mechanics and Engineering*, Vol. 198 Nos 5-8, pp. 838-852.

Cussler, E.L. (2013), "Multicomponent diffusion", *Chemical Engineering Monographs*, Vol. 3. Elsevier Science, New York, NY.

Fisher, R.A. (1937), "The wave of advance of advantageous genes", *Annals of Eugenics*, Vol. 7 No. 4, pp. 355-369.

Garvie, M.R., Burkardt, J. and Morgan, J. (2015), "Simple finite element methods for approximating predator–prey dynamics in two dimensions using Matlab", *Bulletin of Mathematical Biology*, Vol. 77 No. 3, pp. 548-578.

Grünbaum, D. (1999), "Advection-diffusion equations for generalized tactic searching behaviors", *Journal of Mathematical Biology*, Vol. 38 No. 2, pp. 169-194.

Hughes, T.J.R. (1995), "Multiscale phenomena: Green's functions, the Dirichlet-to-Neumann formulation, subgrid scale models, bubbles and the origins of stabilized methods", *Computer Methods in Applied Mechanics and Engineering*, Vol. 127 Nos 1-4, pp. 387-401.

Hughes, T.J.R., Feijóo, G.R., Mazzei, L. and Quincy, J.-B. (1998), "The variational multiscale method – a paradigm for computational mechanics", *Computer Methods in Applied Mechanics and Engineering*, Vol. 166 Nos 1/2, pp. 3-24, Advances in Stabilized Methods in Computational Mechanics.

Linares-Barranco, B., Sánchez-Sinencio, E., Rodríguez Vázquez, A. and Huertas, J.L. (1991), "A CMOS implementation of FitzHugh-Nagumo neuron model", *IEEE Journal of Solid-State Circuits*, Vol. 26 No. 7, pp. 956-965.

Malchow, H. (2008), *Spatiotemporal Patterns in Ecology and Epidemiology: theory, Models, and Simulation*, Chapman and Hall/CRC Press, Boca Raton.

Medvinsky, A.B., Petrovskii, S.V., Tikhonova, I.A., Malchow, H. and Li, B.-L. (2002), "Spatiotemporal complexity of plankton and fish dynamics", *SIAM Review*, Vol. 44 No. 3, pp. 311-370.

Murray, J.D. (2007), *Mathematical Biology: I. An Introduction*, Springer, Berlin.

Nagumo, J., Arimoto, S. and Yoshizawa, S. (1962), "An active pulse transmission line simulating nerve axon", *Proceedings of the Ire*, Vol. 50 No. 10, pp. 2061-2070.

Principe, J. and Codina, R. (2010), "On the stabilization parameter in the subgrid scale approximation of scalar convection diffusion reaction equations on distorted meshes", *Computer Methods in Applied Mechanics and Engineering*, Vol. 199 Nos 21/22, pp. 1386-1402.

Ryabov, A.B. and Blasius, B. (2008), "Population growth and persistence in a heterogeneous environment: the role of diffusion and advection", *Mathematical Modelling of Natural Phenomena*, Vol. 3 No. 3, pp. 42-86.

Shigesada, N. and Kawasaki, K. (1997), *Biological Invasions: Theory and Practice*, Oxford University Press, Oxford.

Tikhomirov, V.M. (1991), *Selected Works of A. N. Kolmogorov: Volume I: Mathematics and Mechanics. Mathematics and Its Applications*, Springer, Netherlands.

Zhu, L., Zhao, H. and Wang, H. (2016), "Complex dynamic behavior of a rumor propagation model with spatial-temporal diffusion terms", *Information Sciences*, Vol. 349-350, pp. 119-136.

Corresponding author
Ramon Codina can be contacted at: ramon.codina@upc.edu